Rayleigh Wave Propagation in Curved Waveguides

Dedicated to Jan D. Achenbach

John G. Harris

216 Talbot Laboratory, 104 South Wright St., Urbana, IL 61801

Abstract

A JWKB asymptotic expansion describing inplane elastic waves is used to approximate a Rayleigh-like wave guided within an elastic waveguide whose curvature is small and changes slowly over a wavelength. The two lowest eigenmodes in a curved guide, taken together, constitute the Rayleigh-like wave. It is shown that this wave lies in the shadows of four, closely spaced, virtual caustics, two caustics per constituent eigenmode. If the curvature becomes too large one or more of the caustics ceases to be virtual and enters the guide after which it is not possible for a Rayleigh-like wave to propagate. The Rayleigh-like wave is dispersive. The dispersion is caused by the constraint that it be confined within the guide, but may also be caused by the curvature alone. For propagation in a thin curved guide, the dispersion caused by the confinement is calculated. The possibility that dispersion may also caused by the curvature alone is not resolved. For a thick guide the effect of confinement is eliminated. In this case it is shown that dispersion caused by a linear dependence of the wavenumber on the curvature is present. Propagation into an environment of increasing curvature is studied, for both waveguides, to exhibit the influence of the nearby caustics.

Key words: Rayleigh waves, surface waves, curved waveguides, caustics

1 Introduction

The character of guided waves in a curved waveguide depends very critically upon whether or not a caustic forms within the guide itself [1]. Figure 1 shows a curved elastic waveguide. We imagine that its inplane eigenmodes — ones that for small curvature are very similar to the Rayleigh-Lamb eigenmodes of

Email address: jgharris@uiuc.edu (John G. Harris).

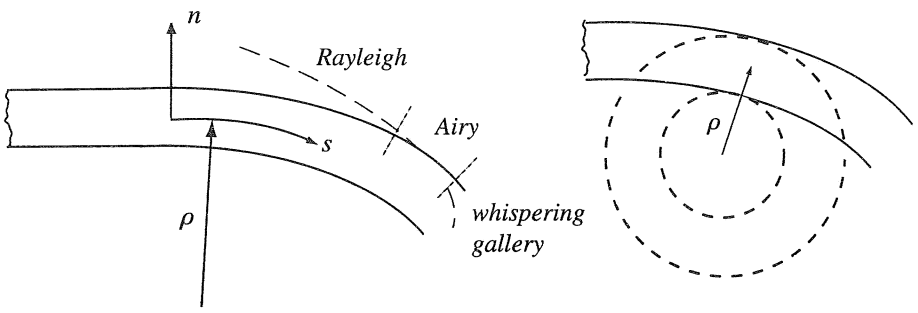

Fig. 1. A drawing describing the problem. The dimensioned curvilinear coordinates are (s, n). s is the arc length along the center line of the guide, n the normal distance from the center line and ρ the variable radius of curvature. The dashed line indicates one of the caustics that is induced by the curvature. The annulus whose radii of curvature match those of the two surfaces of the curved waveguide at a particular point x is shown on the right.

an elastic plate — propagate to the right into a region of increasing curvature. At high frequences and for small curvature, the sum of the two lowest eigenmodes in the curved guide combine to form a Rayleigh-like wave. However, in contrast to propagation in an elastic plate, accompanying these two lowest eigenmodes are four closely spaced caustics induced by the curvature. Two caustics accompany each eigenmode: one accompanies the compressional component and one the shear component. Provided the curvature remains small the caustics form beyond the concave surface of the guide. However, as the curvature increases one or more of the caustics soon enters the guide. One such caustic is indicated in Fig. 1 by the dashed line. The Rayleigh-like wave can propagate only if the caustics accompanying its constituent eigenmodes remain beyond the concave surface. When the caustics have entered the guide the eigenmodes have transformed into ones that are of a whispering gallery type. In Fig. 1 the two propagation regions are labelled *Rayleigh* and *whispering gallery*, with the transition region, where the caustics intersect the concave surface, labelled *Airy*. The principal reason for undertaking the calculations described in this paper is to study the propagation of the Rayeligh-like wave in the Rayleigh region, and to understand how its caustics limit its propagation. While the curvature there must be small, cases of small curvature (small when appropriately scaled) are commonly encountered in ultrasonic nondestructive testing, where the frequencies used are on the order of a megahertz.

At least two asymptotic approaches to this type of problem have been proposed. One approach, a ray theory, uses an approximation constructed from a phase term multiplying an expansion in inverse powers of the wavenumber. This is used in the work of Grimshaw [2] to study surface waves guided by a curved boundary. The boundary is endowed with an impedance boundary condition that allows surface waves to exist. It is also used in the work of Gregory [3] to study Rayleigh waves propagating over a three-dimensional, arbitrarily curved surface. A second approach uses a JWKB approximation

in the direction of propagation along the length of the guide, but a modal representation to describe the behavior of the wavefields at each cross-section. This approach has been taken by Smith, [4] and [5], to describe various guided waves including acoustical whispering gallery waves and sound waves propagating in a slowly curved guide. It is also used by Burridge and Weinberg [6] to study underwater sound waves in an inhomogeneous propagation environment. A second reason for undertaking the calculations of this paper is to show that this latter approach using rays and eigenmodes more successfully represents guided waves, including surface waves, than does the ray theory.

Surface waves propagating in curved structures have been extensively studied in a variety of other ways and contexts. Krylov [7] develops an asymptotic description of Rayleigh waves propagating over a curved surface that is similar to the ray-mode construction previously noted. Viktorov [8] and Rulf [9] study Rayleigh waves on both convex and concave circular surfaces. Beginning with the exact solutions, they pay particular attention to the change in wavenumber caused by the curvature. Brekhovskikh [10] studies both Rayleigh and whispering gallery waves in a solid cylinder using an approximate approach that is too coarse to capture the correction to the Rayleigh wavenumber induced by the curvature. Using a boundary-layer analysis, Morrison [11] studies surface waves, supported by an impedance boundary condition, propagating along an edge whose cross-section curves away rapidly on each side, while Wilson and Morrison [12] follow this with a study of Rayleigh waves propagating along a similar edge in a solid.

There has been less work done on propagation in curved waveguides where the waves are constrained to propagate within the structure rather than be guided by a single surface. As indicated previously, Smith [5] studies scalar propagation in a slowly curving guide, but does not appear to encounter difficulties with caustics forming within the guide. Ahluwalia *et al.* [13] also consider scalar propagation in a slowly curving guide with impedance boundary conditions at the walls. The two approaches indicated previously are used. The second approach, called by the authors the boundary layer method, is used to examine propagation in the guide when the caustic forms within it. This work is followed by a second paper [14] in which the boundary layer method is used to expand upon the parts of the work found in the first, though here the emphasis is upon describing the eigenmodes of a concave body. Work similar to that found in this second paper is also described in Babič and Kirpičnikova [15] and, much more extensively, though somewhat differently, in Babič and Buldyrev [16].

One of the few studies of inplane elastic waves in curved waveguides are those undertaken by Liu and Qu, [17] and [18]. They undertake a partially analytic and partially numerical analysis of propagation in a solid annulus. By enforcing periodic boundary conditions in the angular coordinate, they pose the problem

as one of vibration, rather than propagation. In the course of their work they calculate numerically the exact dispersion relation for an annulus and make the important observation that, at higher frequencies, it is very similar to the Rayleigh-Lamb dispersion relations for an elastic plate.

The problem discussed here is initially formulated as a system of four coupled differential equations exactly as was done by Folguera and Harris [19] when examining coupled Rayleigh waves in a plate of variable thickness. This formulation allows us to describe as rays the propagation along the length of the curved guide and as eigenmodes (or eigenvectors) the wavefield at each cross-section. It leads to an asymptotic expansion in two dimensionless small parameters: the scaled curvature and the scaled rate of change of that curvature over a wavelength. These two small parameters are independent of one another. This choice of parameters contrasts with that taken in most of the asymptotic calculations described previously, where it is assumed that the inverse of the wavenumber is the only small parameter. We use the eigenmodes for an annulus whose radii of curvature correspond to those of the curved guide at the particular position being examined. The figure to the right in Fig. 1 illustrates this. The underlying eigenvalue problem is described by Bessel's equation. We seek asymptotic solutions to this problem on the assumption that the curvature is small. This is equivalent to seeking asymptotic approximations to Hankel functions whose argument and order are both large. Such approximations are attributed to Debye [20].

As the calculation proceeds we discover that the underlying difficulty is not with finding a possible asymptotic solution, but with completing the solution by satisfying the boundary conditions and thus finding the dispersion relation. A third reason for undertaking the work of this paper is to calculate approximate analytical results. To do so, we thus must consider, not the general case, but two special cases: a thin guide and a thick one. For the thin guide we calculate the dispersion caused by the confinement of the wavefield within the guide, but are unable to calculate a possible correction to the dispersion caused by the curvature alone. As might be expected, the thick guide supports a Rayleigh wave on only one surface, which we take to be the concave one, while the other surface is not sensed. In this case, we calculate the correction to the wavenumber caused by the curvature.

2 Formulation

2.1 The equations of motion without mixed derivatives

Figure 1 illustrates the geometry and defines the dimensioned coordinates of the problem. Note that s is the arc length along the center line of the guide and that the positive sense of n is toward the concave (outer) surface. The asymptotic expansion is one in two dimensionless parameters: δ the rate at which the curvature changes over a wavelength and χ the scaled curvature[1]. The dimensionless coordinates and geometrical parameters are defined as

$$x = \delta k_T s, \;\; z = k_T n, \;\; \chi = 1/(k_T \rho), \;\; h = k_T H,$$

where k_T is the shear-wave wavenumber, ρ the radius of curvature of the center line of the guide and H one-half the thickness of the guide. The dimensionless curvature χ is a function of x, though this dependence is not always explicitly exhibited. It is readily seen that

$$[\chi(x + \delta 2\pi) - \chi(x)]/2\pi \approx \delta d\chi/dx.$$

Hence, provided the derivative is no more than O(1), δ measures the rate of change of the curvature over a wavelength. We work in that part of the parameter space where both δ and χ are small.

The equations of motion are written in such a way that no mixed derivatives appear. To achieve this we work with a four dimensional vector having as its components the scaled particle displacements u_1 and u_2, and the scaled stress components τ_1 and τ_2. These terms are related to their dimensioned counterparts by

$$u_1 = k_T u_s, \;\; u_2 = k_T u_n, \;\; \tau_1 = \tau_{ss}/\mu, \;\; \tau_2 = \tau_{sn}/\mu.$$

The vector

$$\mathbf{U} := [u_1, u_2, \tau_1, \tau_2]^T, \tag{1}$$

where the superscript T indicates the transpose.

The Lamé constants λ and μ are combined in the ratio κ_{LT}, which is given by

$$\kappa_{LT} = \frac{c_L}{c_T} = \left(\frac{\lambda + 2\mu}{\mu}\right)^{1/2},$$

[1] We modify this somewhat when the eigenvalue problem is discussed. The parameter used there is $1/\nu = \chi/\beta_p$. We have yet to introduce β_p.

where c_L and c_T are the compressional and shear wavespeeds, respectively. Moreover, it is convenient to introduce the following three interrelated constants, namely,

$$a = [1 - (2/\kappa_{LT}^2)], \quad b = \kappa_{LT}^{-2}, \quad c = 4(a+b).$$

We write the equations of motion for inplane elastic waves, in the coordinates (x, z), as

$$(\mathcal{L} - \delta\partial_x)\,\mathbf{U} = 0. \tag{2}$$

The operator $\mathcal{L}$ is defined by

$$\mathcal{L} := \begin{bmatrix} 0 & -a(1+\chi z)\partial_z - \chi & b(1+\chi z) & 0 \\ -(1+\chi z)\partial_z + \chi & 0 & 0 & (1+\chi z) \\ -(1+\chi z) & 0 & 0 & -(1+\chi z)\partial_z - 2\chi \\ 0 & -c\partial_z[(1+\chi z)\partial_z] - (1+\chi z) & -a(1+\chi z)\partial_z + 2b\chi & 0 \end{bmatrix}. \tag{3}$$

The boundary conditions demand that the traction on each surface vanish. These are written in terms of the components of $\mathbf{U}$, which is given by (1), as

$$c\partial_z u_2 + a\tau_1 = 0, \quad \tau_2 = 0, \tag{4}$$

and are imposed at $z = \pm h$. This particular way of writing the equations for inplane elastic waves was suggested by the work of Kirrmann [21].

2.2 An outline of the asymptotic method

Equations (1) – (4) give a convenient symbolic representation of the equations of motion. Continuing with this representation, we assume that the solution may be asymptotically expanded as

$$\mathbf{U}(x,z) \sim e^{i\Theta(x)/\delta} \sum_{n\geq 0} \mathbf{U}_n(x,z)\delta^n. \tag{5}$$

Setting

$$d\Theta/dx = \beta_p(x), \tag{6}$$

we are led to the following recursive system:

$$\mathcal{L}\mathbf{U}_n - i\beta_p \mathbf{U}_n = \partial_x \mathbf{U}_{n-1}, \tag{7}$$

where terms with negative subscripts are zero. The leading equation is

$$\mathcal{L}\mathbf{U}_0 - i\beta_p \mathbf{U}_0 = 0.$$

Setting $\mathbf{U}_0 = a_0^p(x)\mathbf{u}_p$ we are led to

$$\mathcal{L}\mathbf{u}_p - i\beta_p \mathbf{u}_p = 0, \tag{8}$$

where the operator $\mathcal{L}$ is given by (3). When combined with the boundary conditions (4), this defines an eigenvalue problem with the lateral wavenumber β_p as the eigenvalue. For the moment let us assume that we have solved this problem and have found a complete set of eigenvectors $\mathbf{u}_p$.

To formulate an orthogonality relation we use the bilinear form

$$\langle \mathbf{U}, \mathbf{V} \rangle = -i \int_{\mathcal{R}} \left(u_1^* \sigma_1 + u_2^* \sigma_2 - v_1 \tau_1^* - v_2 \tau_2^* \right) dz, \tag{9}$$

where $\mathbf{U} = [u_1, u_2, \tau_1, \tau_2]^T$ and $\mathbf{V} = [v_1, v_2, \sigma_1, \sigma_2]^T$. The * indicates the complex conjugate. The interval of integration $\mathcal{R}$ is $[-h, h]$ for the waveguide we are presently considering. Note that this definition is the complex conjugate of the one given by equation (3.7) of [19]. Using this, we may derive the following integration by parts formula:

$$\begin{aligned} &\langle \mathbf{V}, \mathcal{L}\mathbf{U} \rangle + \langle \mathcal{L}\mathbf{V}, \mathbf{U} \rangle \\ &\qquad = i \left\{ (1 + \chi z) \left[(v_1^* \tau_2 - u_1 \sigma_2^*) + a(v_2^* \tau_1 - u_2 \sigma_1^*) \right.\right. \\ &\qquad\qquad \left.\left. + \, c(v_2^* \partial_z u_2 - u_2 \partial_z v_2^*) \right] \right\} |_{\partial \mathcal{R}}, \end{aligned} \tag{10}$$

where $\partial\mathcal{R}$ indicates the end points of the interval of integration, $\pm h$ in the present case. If the boundary conditions (4) are satisfied by both vectors, then the right-hand side is zero, indicating that the operator $\mathcal{L}$ is skew symmetric. The two eigenvectors $\mathbf{u}_n$ and $\mathbf{u}_m$ satisfy the boundary conditions. It follows then that

$$i(\beta_n - \beta_m^*) P_{mn} = 0, \tag{11}$$

where

$$P_{mn} := \langle \mathbf{u}_m, \mathbf{u}_n \rangle. \tag{12}$$

Therefore, for $\beta_n \neq \beta_m^*$, $P_{mn} = 0$, and $\mathbf{u}_n$ and $\mathbf{u}_m$ are orthogonal.

The higher order vectors $\mathbf{U}_n$ are expanded as

$$\mathbf{U}_n = \sum_{q \geq 0} a_n^q(x)\mathbf{u}_q, \tag{13}$$

where $a_n^q = \langle \mathbf{u}_m, \mathbf{U}_n \rangle$ when $\beta_q = \beta_m^*$. Therefore a knowledge of the a_n^q gives the higher order $\mathbf{U}_n$. We do not calculate the higher order terms in this work.

It remains to determine the amplitude term $a_0^p(x)$ introduced immediately preceding (8). To do so we work with (7) for $n = 1$. Using $\mathbf{U}_0 = a_0^p\mathbf{u}_p$, this can be written as

$$\mathcal{L}\mathbf{U}_1 = i\beta_p\mathbf{U}_1 + (da_0^p/dx)\mathbf{u}_p + a_0^p\partial_x\mathbf{u}_p.$$

We also consider

$$\mathcal{L}\mathbf{u}_m = i\beta_m\mathbf{u}_m.$$

Using (10) we form the product of the first equation with $\mathbf{u}_m$ and of the second with $\mathbf{U}_1$. Next we combine the two to form

$$(da_0^p/dx)\langle \mathbf{u}_m, \mathbf{u}_p \rangle + a_0^p\langle \mathbf{u}_m, \partial_x\mathbf{u}_p \rangle + i(\beta_p - \beta_m^*)a_1^q = 0. \tag{14}$$

Setting $\beta_p = \beta_m^*$ gives an equation for $a_0^p(x)$. Interchanging p and m and taking the complex conjugate gives a similar equation for a_0^{m*}. Combining these two equations and integrating gives

$$a_0^{m*}(x)a_0^p(x) = C_{mp}^2/P_{mp}(x),$$

where $\beta_p = \beta_m^*$, P_{mp} is given by (12) and C_{mp} is a constant. Keep in mind that the eigenvalue problem represented by (8) is solved at each position x along the guide. Therefore the eigenvectors $\mathbf{u}_p$ will depend not only on z but also on x. Thus P_{mp} depends on x. This result is the adiabatic relation for this problem and expresses the slow variation of the amplitude as a consequence of the slow variation in curvature.

For the case we encounter in this paper the eigenvalues are real so that $m = p$ and

$$|a_0^p(x)| = C_{pp}/P_{pp}^{1/2}(x). \tag{15}$$

By setting $a_0^p = |a_0^p|e^{i\varphi_0^p}$ and returning to (14), we obtain an equation for the argument φ_0^p that is readily integrated. Thus, we find that

$$a_0^p(x) = \frac{C_{pp}}{P_{pp}^{1/2}(x)} \exp\left[-i\int_0^x \frac{\Im\left(\langle \mathbf{u}_p, \partial_x\mathbf{u}_p \rangle\right)}{P_{pp}}\right] d\xi, \tag{16}$$

where P_{pp} is defined by (12).

2.3 Remarks

1. The above outline depends upon their being a complete set of eigenvectors. We assume in this paper that the eigenvectors or eigenmodes that we find do form a complete set, trusting that provided our answers make physical sense and reduce to know results that our methods are accurate.

2. In [19] all the coefficients $a_n^q(x)$ for a problem similar to the one being considered here are found, allowing all the $\mathbf{U}_n$ to be constructed by expanding them as indicated in (13). If the eigenvalues for any two eigenvectors are close to one another (see equation (3.29) of [19]) then the corresponding $a_n^q(x)$. become very large indicating that the asymptotic expansion in δ has become disordered. If these eigenvalues differ by 2ϵ then the term of concern is of the order $\delta/(2\epsilon)$. This possibility arises here. In the next section we calculate and then combine the two lowest eigenmodes for the curved waveguide. The two eigenvalues for these eigenmodes are quite close and both approximate that for a Rayleigh wave. However, in this problem δ must be very small, because we cannot let the curvature increase very much. If we do, one of the caustics enters the guide and Rayleigh wave propagation ceases. Hence this is not a serious limitation for the work of this paper. Nevertheless, perhaps in another context, this issue requires further investigation, especially as these two eigenmodes coalesce to form a single eigenmode.

3 The eigenvalue problem

3.1 Expressed in terms of potentials

The eigenvalue problem that we must solve is that of finding the eigenvectors or eigenmodes of an annulus whose two radii of curvature match those of the two surfaces of the waveguide at a given position x along the guide. This idea is illustrated in right-hand figure in Fig. 1. However, it is not convenient to solve the problem using the form given by (8). Instead we reduce the problem to one in terms of potentials. Firstly, we introduce a new coordinate r and a new parameter ν given by

$$r = [1 + \chi(x)z]/\beta_p, \quad \nu = \beta_p/\chi(x). \tag{17}$$

The parameter ν is very large. Though seeking the pth eigenvector we do not indicate the p unless it is needed. Note that β_p may depend upon χ. Secondly, we eliminate the τ_1 and τ_2 from (8) and introduce the potentials φ and ψ

through the relations

$$u_1 = \frac{i}{r}\varphi + \frac{1}{\nu}\frac{d\psi}{dr}, \quad u_2 = \frac{1}{\nu}\frac{d\varphi}{dr} - \frac{i}{r}\psi.$$

Note x is fixed for the moment (though not absent), so that in place of ∂_r we use d/dr. Thirdly, we find that the potentials satisfy

$$\frac{1}{\nu^2}\frac{d}{dr}\left(r\frac{d\varphi}{dr}\right) + \frac{1}{r}\left(\frac{r^2}{\kappa_{LT}^2} - 1\right)\varphi = 0, \quad \frac{1}{\nu^2}\frac{d}{dr}\left(r\frac{d\psi}{dr}\right) + \frac{1}{r}\left(r^2 - 1\right)\psi = 0. \tag{18}$$

Lastly, we express the boundary conditions (4) as

$$\frac{i}{r}u_2 - \frac{1}{\nu r}u_1 + \frac{1}{\nu}\frac{du_1}{dr} = 0, \quad \frac{1}{\nu}\frac{du_2}{dr} + \frac{ia}{r}u_1 + \frac{a}{\nu r}u_2 = 0. \tag{19}$$

Equations (18) are Bessel's equations and have solutions formed from a combination of $H_\nu^{(1,2)}(\nu r/\kappa_{LT})$ and one of $H_\nu^{(1,2)}(\nu r)$. ν is large, while r is fixed. We therefore use the Debye approximation [20] to the Hankel functions. To have a Rayleigh-like wave in the guide, we require that the Hankel functions have increasing or decreasing exponential behavior. Therefore we ask that $(r/\kappa_{LT}) < 1$ and $r < 1$. From our knowledge of the Rayleigh-Lamb eigenmodes in a plate, we suspect that the eigenmodes that we seek have a limited degree of reflection symmetry or antisymmetry, with respect to the center line of the guide. We arrange the arguments to capture this feature. This leads us to asymptotic approximations [2] to the potentials and then to those for the particle displacements. The approximate particle displacements are

$$u_1^{a,s} \sim \frac{i\,C_L^{a,s}}{rR_L^{1/2}}\begin{pmatrix}\sinh[\nu(S_L - S_{mL})]\\ \cosh[\nu(S_L - S_{mL})]\end{pmatrix} + \frac{C_T^{a,s}R_T^{1/2}}{r}\begin{pmatrix}\sinh[\nu(S_T - S_{mT})]\\ \cosh[\nu(S_T - S_{mT})]\end{pmatrix}, \tag{20}$$

and

$$u_2^{a,s} \sim \frac{C_L^{a,s}R_L^{1/2}}{r}\begin{pmatrix}\cosh[\nu(S_L - S_{mL})]\\ \sinh[\nu(S_L - S_{mL})]\end{pmatrix} - \frac{i\,C_T^{a,s}}{rR_T^{1/2}}\begin{pmatrix}\cosh[\nu(S_T - S_{mT})]\\ \sinh[\nu(S_T - S_{mT})]\end{pmatrix}, \tag{21}$$

as $\nu \to \infty$. Note how the arguments of the cosh and sinh are arranged to give the reflection symmetry referred to previously. The superscripts a and s indicate antisymmetric and symmetric respectively. The superscript a corresponds to the upper term in the parenthesis and the superscript s to the lower

[2] A more informative way to proceed is to seek directly JWKB solutions to (18).

one. The several ancillary expressions are

$$S_L(r) = R_L(r) - \cosh^{-1}\left(\frac{\kappa_{LT}}{r}\right), \quad S_T(r) = R_T(r) - \cosh^{-1}\left(\frac{1}{r}\right), \tag{22}$$

with

$$R_L(r) = \left(1 - \frac{r^2}{\kappa_{LT}^2}\right)^{1/2}, \quad R_T(r) = \left(1 - r^2\right)^{1/2}, \tag{23}$$

and

$$S_{mI} = \frac{1}{2}[S_I(r_+) + S_I(r_-)], \tag{24}$$

where $I = L, T$. Further

$$r_\pm = (1 \pm \chi(x)h)/\beta_p. \tag{25}$$

The remaining issue is to satisfy the boundary conditions (19), determine the eigenvalue β_p and determine the ratios $C_T^{a,s}/C_L^{a,s}$. We anticipate finding two eigenvalues, β_a and β_s. This is not easily done. We immediately find that the eigenmodes of both reflection symmetries are coupled together by the boundary conditions. There are two cases that admit some degree of analytical approximation. The first is a thin, shallowly curved guide for which $\chi(x)h < 1$ and the second is one for which h is so great that the wave becomes a Rayleigh wave on one of the surfaces, never sensing the opposite one.

3.2 Remarks

1. Note that the expressions become unbounded when $r = \kappa_{LT}$ or $r = 1$. These locate the caustics for the compressional and shear components, respectively, of the eigenmodes of the approximating annulus at x. As the annulus is rolled along x, their envelopes trace out the caustics for the curved guide, one of which is sketched in Fig. 1. As indicated in the introduction the various regions have different asymptotic characters and in general we should need to use uniform approximations to the Hankel functions to capture the character of the wavefields in Airy region.

2. To remain in the Rayleigh region the criteria hardest to satisfy is $r < 1$. This implies that $\chi(x)h < (\beta_p - 1)$, $\forall x$ in the range of interest. For a Rayleigh-like wave $\beta_p \approx 10/9$ so that $\chi(x)h < 1/10, \forall x$. Moreover, we ask that $\delta << 1$ so that $\chi(x)$ does not become too large as x increases. *Therefore, the impending intersection of the nearest caustic with the concave surface sets the basic limits to our calculation of Rayleigh-like waves in curved guide.* Even when h becomes

very large, this limitation does not go away, though it does take a different form, which fact we investigate in §5.

4 A thin, shallowly curved guide

4.1 The eigenvalues and eigenvectors

To impose the boundary conditions (19), we define four ancillary functions that are effectively slowly-varying amplitude terms. These are

$$A_L(r) = \frac{1}{bR_L^{1/2}}\left(\frac{R_L^2}{r^2} - \frac{a}{r^2}\right), \qquad A_T(r) = -\frac{i\,2R_T^{1/2}}{r^2},$$
$$B_L(r) = \frac{i\,2R_L^{1/2}}{r^2}, \qquad B_T(r) = \frac{1}{R_T^{1/2}}\left(\frac{R_T^2}{r^2} + \frac{1}{r^2}\right). \tag{26}$$

We next introduce the following abbreviations:

$$Cd_I = \cosh\left\{(\nu/2)[S_I(r_+) - S_I(r_-)]\right\}, \quad Sd_I = \sinh\left\{(\nu/2)[S_I(r_+) - S_I(r_-)]\right\},$$

and

$$A_{I\pm} = A_I(r_+) \pm A_I(r_-), \quad B_{I\pm} = B_I(r_+) \pm B_I(r_-),$$

where $r_\pm$ is given by (25) and $I = L, T$. Direct imposition of (19) indicates that we must use both eigenmodes to satisfy the boundary conditions because of the asymmetry about the center line. However, by examining the arguments of the sinh and cosh terms, we observe that, by adding and subtracting, the boundary conditions, they can be expressed as

$$\begin{bmatrix} A_{L+}\,Sd_L & A_{T+}\,Sd_T & A_{L-}\,Cd_L & A_{T-}\,Cd_T \\ B_{L+}\,Cd_L & B_{T+}\,Cd_T & B_{L-}\,Sd_L & B_{T-}\,Sd_T \\ A_{L-}\,Sd_L & A_{T-}\,Sd_T & A_{L+}\,Cd_L & A_{T+}\,Cd_T \\ B_{L-}\,Cd_L & B_{T-}\,Cd_T & B_{L+}\,Sd_L & B_{T+}\,Sd_T \end{bmatrix} \begin{bmatrix} C_L^a \\ C_T^a \\ C_L^s \\ C_T^s \end{bmatrix} = \begin{bmatrix} 0 \\ 0 \\ 0 \\ 0 \end{bmatrix}. \tag{27}$$

Expanding the amplitude terms $A_{I\pm}, B_{I\pm}$ about the centerline $z = 0$ in powers of h/ν, we note that those with a $-$ sign as a subscript are $\mathrm{O}(h/\nu)$. Therefore, to order $\mathrm{O}[(h/\nu)^2]$, the determinant of this system vanishes if the smaller determinants formed from the upper left and lower right 2×2 submatrices vanish. This gives us antisymmetric and symmetric dispersion relations little different from those for the antisymmetric and symmetric Rayleigh-Lamb

eigenmodes for a flat plate. This agrees with the observation in [17], noted previously. Moreover, we obtain the ratios C_T^a/C_L^a and C_T^s/C_L^s, at least to $O(h/\nu)$, independently from one another. Thus we end with two uncoupled eigenmodes and may state that the curvature couples the two lowest eigenmodes of the curved waveguide to $O[(h/\nu)^2]$.

We expect, from a knowledge of the behavior of the two lowest Rayleigh-Lamb eigenmodes of a plate, that $\beta_p \approx \beta_r \pm \epsilon$, where β_r is the scaled Rayleigh wavenumber for a half-space and ϵ is a small correction. The specific calculation of the two β_p's and the two approximate eigenmodes parallels that in §3(b) of [19]. The only additional step is to note that

$$S_I(r_+) - S_I(r_-) = 2h\frac{dS_I}{dr}(1/\beta_{a,s}) + O[(h/\nu)^2], \tag{28}$$

for $I = L, T$. The outcomes are the following. The eigenvalues β_a and β_s are given by

$$\beta_{a,s} \approx \beta_r \pm \epsilon, \tag{29}$$

where

$$\beta_r = \frac{c_T}{c_r}, \quad \frac{c_T}{c_r} \approx \frac{4 - 3\kappa_{LT}^2}{3.98 - 2.86\kappa_{LT}^2}, \tag{30}$$

and

$$\epsilon = \left| 2\left(\frac{df_r}{d\beta}\bigg|_{\beta_r}\right)^{-1} \left[p^2(e^{-2|\gamma_L|h} - e^{-2|\gamma_T|h}\right]_{\beta_r} \right|. \tag{31}$$

In (29), the + accompanies the subscript a, and the − accompanies the s. The approximation to c_T/c_r is taken from Auld [22]. The function $f_r(\beta)$ is the Rayleigh function given by

$$f_r(\beta) = p^2 - |\gamma_L||\gamma_T|, \tag{32}$$

with

$$\gamma_L(\beta) = [(1 - \kappa_{LT}^2\beta^2)^{1/2}]/\kappa_{LT}, \;\; \gamma_T(\beta) = (1 - \beta^2)^{1/2}, \;\; p(\beta) = (2\beta^2 - 1)/2\beta. \tag{33}$$

Again it is convenient to introduce the several abbreviations:

$$Sa_I = \frac{\sinh\{\nu[S_I(r) - S_{mI}]\}}{\cosh(|\gamma_I|h)}, \quad Ca_I = \frac{\cosh\{\nu[S_I(r) - S_{mI}]\}}{\cosh(|\gamma_I|h)},$$
$$Ss_I = \frac{\sinh\{\nu[S_I(r) - S_{mI}]\}}{\sinh(|\gamma_I|h)}, \quad Cs_I = \frac{\cosh\{\nu[S_I(r) - S_{mI}]\}}{\sinh(|\gamma_I|h)}.$$

The eigenvectors or eigenmodes, to $O(\nu^{-1})$, are given by

$$\mathbf{u}_a \sim \frac{C_a}{\beta_a r}\begin{bmatrix} \left(\dfrac{|\gamma_L|}{\beta_a R_L}\right)^{1/2} Sa_L - \dfrac{|\gamma_L||\gamma_T|}{\beta_a\, p}\left(\dfrac{\beta_a R_T}{|\gamma_T|}\right)^{1/2} Sa_T \\ \left(\dfrac{-i|\gamma_L|}{\beta_a}\right)\left[\left(\dfrac{\beta_a R_L}{|\gamma_L|}\right)^{1/2} Ca_L - \left(\dfrac{\beta_a}{p}\right)\left(\dfrac{|\gamma_T|}{\beta_a R_T}\right)^{1/2} Ca_T\right] \end{bmatrix}, \tag{34}$$

and

$$\mathbf{u}_s \sim \frac{C_s}{\beta_s r}\begin{bmatrix} \left(\dfrac{|\gamma_L|}{\beta_s R_L}\right)^{1/2} Cs_L - \dfrac{|\gamma_L||\gamma_T|}{\beta_s\, p}\left(\dfrac{\beta_s R_T}{|\gamma_T|}\right)^{1/2} Cs_T \\ \left(\dfrac{-i|\gamma_L|}{\beta_s}\right)\left[\left(\dfrac{\beta_s R_L}{|\gamma_L|}\right)^{1/2} Ss_L - \left(\dfrac{\beta_s}{p}\right)\left(\dfrac{|\gamma_T|}{\beta_s R_T}\right)^{1/2} Ss_T\right] \end{bmatrix}. \tag{35}$$

Each term in (34) is evaluated with $\beta_p = \beta_a$ and each one in (35) with $\beta_p = \beta_s$. S_I, R_I, S_{mI} and r are given by (22), (23), (24) and (17), respectively, and γ_I and p by (33). The $C_{a,s}$ are constants set by a normalization.

4.2 The wavefield

Returning to the results of §2.2 we now calculate the $a_0^p(x)$ given by (16) and the $P_{pp}(x)$ defined by (12), for $p = a, s$. We readily find that

$$\Im\left(\langle \mathbf{u}_p, \partial_x \mathbf{u}_p\rangle\right) = 0.$$

To calculate the $P_{pp}(x)$ we return to the coordinate z and write

$$P_{pp}(x) = 2\int_{-h}^{h} \Im(u_1^{p*}\tau_1^p + u_2^{p*}\tau_2^p)dz,$$

with

$$u_1^{p*}\tau_1^p + u_2^{p*}\tau_2^p = \frac{i\,\beta_p}{1+\chi z}\left(\frac{|u_1^p|^2}{b} + |u_2^p|^2\right) + \left(\frac{a}{b}u_1^{p*}\partial_z u_2^p + u_2^{p*}\partial_z u_1^p\right) + O(\nu^{-1}).$$

Combining the results of the preceding sections gives the total Rayleigh-like wavefield in the thin, curved guide as

$$\mathbf{U}(x,z) \sim \left[\frac{\mathbf{u}_a(x,z)}{P_{aa}^{1/2}(x)}e^{i\epsilon k_T s} + \frac{\mathbf{u}_s(x,z)}{P_{ss}^{1/2}(x)}e^{-i\epsilon k_T s}\right] e^{i\beta_r k_T s}. \tag{36}$$

Though until now we have not always indicated it, the x dependence enters through $\chi(x)$ and thus enters almost everywhere.

4.3 Remarks

1. This calculation has only been carried to leading order. To this order $\beta_{a,s}$ appear to have no direct dependence on χ. Is this the case? That is, does $\beta_{a,s}$ behave as $\beta_{a,s} \sim \beta_r \pm \epsilon + \chi(x)\beta_{a.s\,1}$?

Note: Were s to be measured along the concave surface instead of the center line, then different wavenumbers, say $\alpha_{a,s}$, such that

$$\beta_{a.s} k_T \rho = \alpha_{a.s} k_T (\rho + H)$$

would be needed. In this case $\alpha_{a,s} \approx \beta_{a,s}(1 - \chi h)$. This is *not* the dependence on χ we are referring to.

It is tempting to think that no such term appears because, viewed from within the guide one surface is concave while the other is convex. However, we cannot know this without a detailed calculation of the boundary conditions to the next order, which is quite lengthy because we lose the partial symmetry used to arrive at (27). Interestingly, we note that, even if a $\beta_{a,s\,1}$ is present, it does not alter the approximation (28) and thus does not affect the arguments of the sinh and cosh in (34) and (35) to $\mathrm{O}[(h/\nu)^2]$.

2. In §5 we consider a thick curved guide, where the boundary condition at only one surface needs to be imposed, in order to explore further a dependence of the wavenumber on χ alone. We know from several of the works cited in the *Introduction* that such a dependence is present when only one boundary is engaged, though it is less clear how it arises using the asymptotic approach of this paper.

4.4 Numerical results

Figures 3 and 4 summarize the outcomes of our calculations. We imagine that the Rayleigh-like wave propagates into an environment of increasing curvature. We take the curvature to be given by

$$\chi(x) = \chi_0 + (\chi_{max} - \chi_0)x.$$

For Rayleigh-like waves $r < 1$. Recall from (29) that the smaller wavenumber is β_s. We therefore set $\chi_{max} = (\beta_s - 1)/h$; this is the curvature at which the caustic associated with the shear component of the symmetric eigenmode

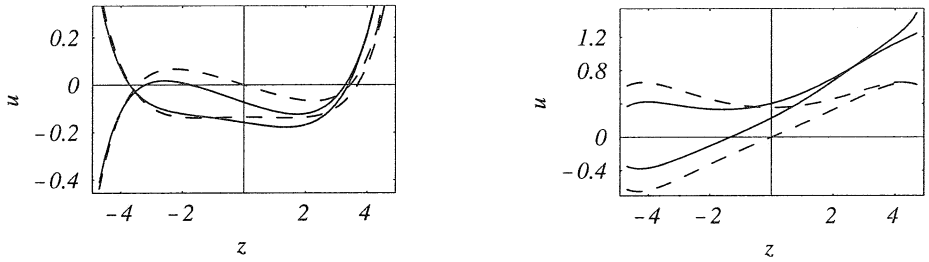

Fig. 2. Shapes of the particle displacements (indicated by u) through the thickness at $x = 0$ and $x = 0.9$. The solid line indicates the particle displacements at $x = 0.9$ and the dashed lines at $x = 0$. The left-hand figure shows the components of $\mathbf{u}_a$ and the right-hand figure those of $\mathbf{u}_s$.

intersects the concave surface. Thus, as x goes from 0 to 1, χ increases to χ_{max}. Recall that x is not the physical distance, but that $x = \delta k_T s$. We take $\delta = \chi_{max}$. We do not want x to go exactly to 1; thus we set its maximum value $x_{max} = 0.9$. With this x_{max}, the maximum physical distance $s_{max} = 0.9/(2\pi\chi_{max})$ shear wavelengths. Lastly, we take $\kappa_{LT} = 1.73$, $h = 4.69$ and $\chi_0 = 0.001$.

Figure 2 shows the variation in the particle displacements (indicated by u) through the thickness at positions where the curvature is a minimum ($x = 0$) and at a position where it is almost a maximum ($x = 0.9$). The solid lines indicate the particle displacements near the position of maximum curvature, while the dashed ones those at that of minimum curvature. In the left-hand figure u_{a1} and u_{a2} are shown. These are given by (34), with $C_a = 1$. The components are identified by noting that u_{a1} is approximately antisymmetric and u_{a2} symmetric about $z = 0$. In the right-hand figure u_{s1} and u_{s2} are shown. These are given by (35), with $C_s = 1$. The components are identified by noting that u_{s1} is approximately symmetric and u_{s2} antisymmetric about $z = 0$. The effect on $\mathbf{u}_s$ (the right-hand figure) of the nearing caustic is very marked.

Equation (36) gives the weighed sum $\mathbf{U}$ of the two eigenmodes. Figure 3 shows the real part of U_2 as x runs from 0 to 0.9. In the left-hand figure $C_a = C_s = 1$ so that the two eigenmodes are launched in-phase. In this figure the solid line indicates U_2 at $z = h$ and dashed one U_2 at $z = 0$. U_2 at $-h$ is too small to be seen on this graph. In the right-hand figure $C_a = -C_s = 1$ so that the two eigenmodes are launched out-of-phase. In this figure the solid line indicates U_2 at $z = -h$ and the dashed one U_2 at $z = 0$. We note in both figures a tendency for the particle displacement to drift toward the concave surface as the point of intersection with the nearest caustic is approached. Though there is a phase difference of $2\epsilon k_T s$ between the two eigenmodes that may enhance this effect,

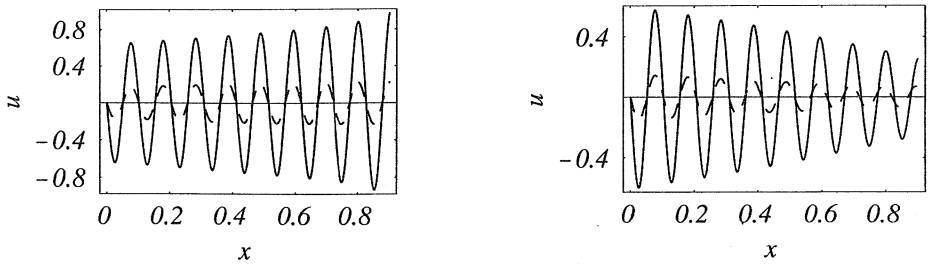

Fig. 3. The real part of U_2 (indicated by u) plotted against x. The left-hand figure shows U_2 when the two eigenmodes are launched in-phase and the right-hand figure that when launched π radians out-of-phase. The solid line indicates U_2 at $z = h$ in the left-hand figure and at $z = -h$ in the right-hand figure. The dashed line indicates U_2 at $z = 0$ in both figures. Note that the vertical scales on the two figures differ.

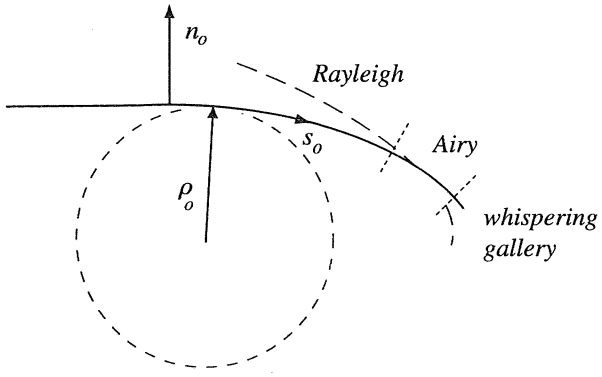

Fig. 4. A drawing of the thick waveguide. The dimensioned curvilinear coordinates are (s_o, n_o). s_o is the arc length along the concave surface of the guide, n_o the normal distance from the surface and ρ_o the variable radius of curvature. The dashed line indicates one of the caustics that is induced by the curvature. The cylinder whose radii of curvature matches that of the concave surface at a particular point x is also shown.

in the case that the Rayleigh-like wave is launched on the convex surface (the right-hand figure), the impending intersection of one of the caustics with the concave surface seems the dominant effect.

5 A thick, shallowly curved guide

5.1 The limit

If we let the convex (lower) surface recede such that the guide becomes very thick we should recover a Rayleigh wave propagating on the concave surface. We consider this possibility, We begin by introducing new curvilinear coordinates (s_o, n_o): s_o measures the distance along the concave surface and n_o measures that normal to the surface. Moreover, we introduce the radius of curvature ρ_o of the concave surface. n_o is positive as one moves outward along the radius of curvature and negative as one moves inward toward the center of curvature. Figure 4 shows the geometry. We next introduce the scaled coordinates and geometrical parameter

$$x_o = \delta k_T s_o, \quad z_o = k_T n_o, \quad \chi_o = 1/(k_T \rho_o).$$

Because we are working with a lateral coordinate that stretches along the surface, rather than along an internal arc, the wavenumber also changes. The new wavenumber α_p is such that

$$\nu = \alpha_p/\chi_o = \beta_p/\chi.$$

Note that ν is unchanged. The coordinate r is now given by

$$r = (1 + \chi_o z_o)/\alpha_p. \tag{37}$$

r is identical to that used previously and is thus also unchanged. At the upper surface $z = 0$, or $r = r_+ = \alpha_p^{-1}$. Taking as the lower surface $z_o = -\chi_o^{-1}$, $r = r_- = 0$. However, χ_o depends on x_o. This would suggest that by allowing the thickness to vary with x_o, as well as does the curvature, we should need to redo completely our analysis. This is not the case. The only place that a variable thickness would enter the calculation is through the boundary conditions as the work of [19] shows. Because the origin of the coordinate system has been moved to the surface $z_o = 0$ the boundary condition does not engage the thickness. Moreover, as $z_o \to -\chi_o^{-1}$ we ask that the wavefield be decaying. Again the boundary condition does not engage the thickness.

We begin by examining the boundary conditions, not in the form (27), but in their original form (19) with the conditions at r_+ separated from those at r_-. We then take a limit as r_- becomes very small. We firstly note that as r_- becomes small

$$\begin{pmatrix} \sinh \nu[S_I(r_+) - S_I(r_-)] \\ \cosh \nu[S_I(r_+) - S_I(r_-)] \end{pmatrix} \sim \frac{1}{2} \left[e^{(\nu/2)S_I(r_+)} \left(\frac{2[\kappa_{LT}]}{r_-} \right)^{\nu/2} \right],$$

where, as in previous instances, $I = L, T$. $[\kappa_{LT}]$ is included when $I = L$, but omitted when $I = T$. Secondly, we note that the amplitude terms (26) behave as

$$A_L(r_-) \sim \frac{2}{r_-^2}, \qquad A_T(r_-) \sim -\frac{i\,2}{r_-^2},$$
$$B_L(r_-) \sim \frac{i\,2}{r_-^2}, \qquad B_T(r_-) \sim \frac{2}{r_-^2}.$$

for r_- small. Thirdly, we define constants $\bar{C}_I^{a,s} := (2/r_-)^{\nu/2} C_I^{a.s}$. Keeping these new constants unchanged as $r_- \to 0$, we find that the boundary conditions are satisfied and the effects of the singular terms in the amplitudes A_I and B_I removed provided $\bar{C}_L^a = \bar{C}_L^s = C_L/(\kappa_{LT})^{\nu/2}$ and $\bar{C}_T^a = \bar{C}_T^s = C_T$. Introducing the new constants C_I, the boundary conditions (19) become

$$\begin{bmatrix} A_L(r_+)\, e^{(\nu/2)S_L(r_+)} & A_T(r_+)\, e^{(\nu/2)S_T(r_+)} \\ B_L(r_+)\, e^{(\nu/2)S_L(r_+)} & B_T(r_+)\, e^{(\nu/2)S_T(r_+)} \end{bmatrix} \begin{bmatrix} C_L \\ C_T \end{bmatrix} = \begin{bmatrix} 0 \\ 0 \end{bmatrix} \tag{38}$$

The vanishing of the determinant gives the Rayleigh equation $f_r(\alpha_p) = 0$, where f_r is given by (32). Thus, to this order of approximation, $\alpha_p = \alpha_r = \beta_r$, the Rayleigh wavenumber. In the next subsection we show that $\alpha_r \sim \beta_r + \chi_o(x_o)\alpha_{r1}$, but at this level of approximation we cannot obtain this correction term.

To find the eigenmode we return to (20) and (21) to carry out the same limiting procedure. Equation (38) then gives the ratio C_T/C_L. The *single* eigenmode is now given by

$$\mathbf{u}_r \sim \frac{C_r}{\beta_r r} \begin{bmatrix} \left(\dfrac{|\gamma_L|}{\beta_r R_L}\right)^{1/2} e^{\nu[S_L(r)-S_L(r_+)]} - \dfrac{|\gamma_L||\gamma_T|}{\beta_r\, p}\left(\dfrac{\beta_r R_T}{|\gamma_T|}\right)^{1/2} e^{\nu[S_T(r)-S_T(r_+)]} \\ -\dfrac{i\,|\gamma_L|}{\beta_r}\left[\left(\dfrac{\beta_r R_L}{|\gamma_L|}\right)^{1/2} e^{\nu[S_L(r)-S_L(r_+)]} - \dfrac{\beta_r}{p}\left(\dfrac{|\gamma_T|}{\beta_r R_T}\right)^{1/2} e^{\nu[S_T(r)-S_T(r_+)]}\right] \end{bmatrix} \tag{39}$$

The S_I are given by (22), the R_I by (23), but r is now given by (37). The γ_I and p are given by (33); $I = L, T$. In S_I, R_I and r (including r_+), $\alpha_r = \beta_r + \chi_o(x_o)\alpha_{r1}$, but in γ_I and p, $\beta = \beta_r$. These choices become apparent when the correction term to α_r, α_{r1} is calculated in the next subsection.

To find a correction to α_r we must examine the boundary conditions to $O(\nu^{-1})$. The boundary condition is now applied at

$$r_+ = 1/[\beta_r + \chi_o(x_o)\alpha_{r1}] \sim r_{+0} - 1/(\nu_o\beta_r),$$

with $r_{+0} = 1/\beta_r$ and $\nu_o = \beta_r/\chi_o$. The $[\nu S_I(r_+)]$, $A_I(r_+)$ and $B_I(r_+)$, (22) and (26) respectively, are expanded to order ν_0^{-1}. We next note that provided the C_I in (38) are replaced by

$$\bar{C}_I = C_I \exp\left\{\frac{1}{2}\left[\alpha_{r1}S_I(r_{+0}) - \frac{\alpha_{r1}}{\beta_r}\frac{dS_I}{dr}(r_{+0})\right]\right\},$$

then (38) continues to be satisfied to leading order. The boundary conditions at order ν_0^{-1} then become

$$\mathbf{AX} = \frac{\alpha_{r1}}{\beta_r}\frac{d\mathbf{A}}{dr}\bar{\mathbf{C}} - \mathbf{B}\bar{\mathbf{C}}. \tag{40}$$

The vector $\mathbf{X}$ contains the amplitude corrections to the potentials ϕ and ψ at order ν_0^{-1}. The vector

$$\bar{\mathbf{C}} = [\bar{C}_L, \bar{C}_T]^T.$$

The matrix $\mathbf{A}$ is the 2×2 matrix on the left-hand side of (38) evaluated at r_{+0}, not r_+. $d\mathbf{A}/dr$ is its derivative evaluated at r_{+0}. Lastly the matrix

$$\mathbf{B} = \begin{bmatrix} D_L(r_{+0})\, e^{(\nu_o/2)S_L(r_{+0})} & D_T(r_{+0})\, e^{(\nu_o/2)S_T(r_{+0})} \\ E_L(r_{+0})\, e^{(\nu_o/2)S_L(r_{+0})} & E_T(r_{+0})\, e^{(\nu_o/2)S_T(r_{+0})} \end{bmatrix}.$$

The several ancillary functions are

$$D_L(r) = \frac{-2R_L^{1/2}}{r^2}, \qquad D_T(r) = \frac{i}{r^2 R_T^{1/2}}\left(2 - \frac{r^2}{R_T^2}\right),$$
$$E_L(r) = \frac{-i}{r^2 R_L^{1/2}}\left(2 - \frac{r^2/\kappa_{LT}^2}{R_L^2}\right), \qquad E_T(r) = \frac{-2R_T^{1/2}}{r^2}. \tag{41}$$

Note that $\det(\mathbf{A}) = 0$. Therefore, for any nontrivial solution $\mathbf{Y}$ to

$$\mathbf{A}^T\mathbf{Y} = 0,$$

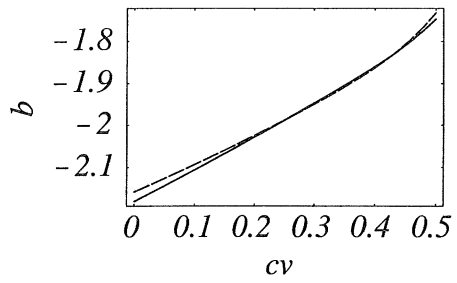

Fig. 5. The correction α_{r1} calculated in this paper, solid line, and that calculated by Gregory [3], dashed line. b symbolizes α_{r1}; cv symbolizes κ_{LT}^{-2}.

then [23],

$$\frac{\alpha_{r1}}{\beta_r}\mathbf{Y}^T\frac{d\mathbf{A}}{dr}\bar{\mathbf{C}} - \mathbf{Y}^T\mathbf{B}\bar{\mathbf{C}} = 0. \tag{42}$$

This gives α_{r1}. This is the consistency condition used by Gregory [3] following his equations (5.7) and (5.8). Note that this condition is similar to that used to obtain an equation for $a_0^q(x)$.

Carrying forward the calculation indicated by (42) gives

$$\frac{\alpha_{r1}}{\beta_r} = \frac{[B_T\, D_T - B_L\, D_T] - [A_T\, E_L - A_L\, E_T]}{[B_T\, d_r A_L - B_L\, d_r A_T] - [A_T\, d_r B_L - A_L\, d_r B_T]}, \tag{43}$$

where d_r means d/dr and each function is evaluated at r_{+0}. The various functions are given by (26) and (41).

Figure 5 shows the correction α_{r1} calculated using (44) as κ_{LT}^{-2} is varied. This is the solid line. The dashed line shows the correction calculated using Gregory's correction D_1 (see equation (6.18) of [3]). The two corrections appear to be identical. The slight discrepancy may arise because the approximation (30) to c_r is used to evaluate both corrections.

5.3 The Rayleigh wave

We now calculate $a_0^r(x_o)$ and $P_{rr}(x_o)$. What our limiting process has shown is that what were formerly two eigenmodes have coalesced to one. In fact the eigenmode we have found is the one that belongs to a solid cylinder whose radius of curvature equals that of the convex surface at a given position x_o. Such a cylinder is sketched in Fig. 4. We now treat the Rayleigh wave as a single mode within a convex body that supports many other eigenmodes, some of which are of a whispering gallery type. We repeat the analysis of §2.2. We set $\mathbf{U}_0 = a_0^r(x_o)\mathbf{u}_r$. The eigenvalue problem becomes the one solved in §5.1 with eigenvalue α_r. The orthogonality relation continues to be given by (14),

except that $\mathcal{R}$ is now $[-\chi_o^{-1}, 0]$. $P_{rr}(x_o)$ continues to be given by (12) and $a_0^r(x_o)$ by (16). Again we find that

$$\Im(\langle \mathbf{u}_r, \partial_x \mathbf{u}_r \rangle) = 0.$$

The Rayleigh wave is now given by

$$\mathbf{U}(x_o, z_o) \sim \frac{\mathbf{u}_r(x_o, z_o)}{P_{rr}^{1/2}(x_o)} \exp[i(\alpha_{r1}/\delta) \int_0^{x_o} \chi_o(\xi) d\xi \,]\, e^{i\beta_r k_T s}. \tag{44}$$

The correction α_{r1} is given by (44).

5.4 Remarks

1. Note that the caustics are still present in the terms R_L and R_T. However, they manifest themselves differently. As before they appear at $r = \kappa_{LT}$ and $r = 1$. Therefore the caustic accompanying the shear component intersects the concave surface at $\chi_{omax} = (1 - \beta_r)/\alpha_{r1}$. To ensure that a Rayleigh wave propagates on a concave surface $\chi_o < \chi_{omax}$. This sets the basic limit to our calculation of Rayleigh wave propagation.

2. We have arrived at the approximating eigenmode by a limiting process that effectively approximates the eigenmode of a convex surface by that of a cylinder of the same radius of curvature (Fig. 4). We then repeated the arguments of §2.2 to arrive at (44). However, this leaves open the question suggested by the second of the *Remarks 2.3*: Just what does happen as eigenmodes coalesce?

3. The case of the convex surface is not treated because any Rayleigh wave on a convex surface must be leaky. The presence of the two caustics within the domain of the guide implies that the Rayleigh wave lies on the shadow side of these caustics. A Rayleigh wave launched on a convex surface must tunnel through its boundary layers reaching the far side of the caustics where it radiates outward.

5.5 Numerical results

Figure 6 summarize the outcomes of our calculations for the thick guide. Again we imagine that the Rayleigh wave propagates into an environment of increasing curvature. We take the curvature to be given by

$$\chi_o(x) = \chi_{o0} + (\chi_{omax} - \chi_{o0}) x_o,$$

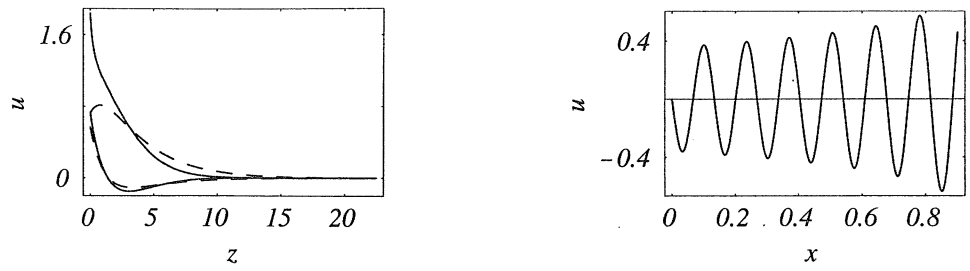

Fig. 6. The left-hand figure shows the two components of the particle displacement for the Rayleigh eigenmode $\mathbf{u}_r$. The solid line indicates the particle displacement at $x = 0.9$ and the dashed one that at $x = 0$. The coordinate z in the figure is $-z_o$. The right-hand figure shows the real part of the component of particle displacement U_{r2} at $z_o = 0$.

where χ_{omax} is given in the first of *Remarks 5.4*. Recall, once again, that x_o is not the physical distance. We now take $\delta = \chi_{omax}$. Moreover we set $x_{omax} = 0.9$. Lastly, we again take $\kappa_{LT} = 1.73$ and $\chi_{o0} = 0.001$.

In Figure 6, the left-hand figure shows the shape of the two components of the eigenmode $\mathbf{u}_r$ given by (39), with $C_r = 1$. Note that the depth coordinate z indicated in the figure equals $-z_o$. The solid line indicates the particle displacement at $x_o = 0,9$, near the position of maximum curvature, while the dashed line indicates that at the position of minimum curvature, $x_o = 0$. The right-hand figure shows the real part of U_{r2} plotted against x_o. As with the thin guide, the impending intersection with one of the caustics dominates the behavior of the Rayleigh wave. The dispersive effect of the correction is not as important as is its role in indicating the intersection of one of the caustics with the concave surface.

6 Closure

An asymptotic framework describing the propagation of inplane elastic waves guided within a slowly curving waveguide has been developed. It gives explicit approximations to the guided waves and is capable of capturing many of the effects induced by the curvature. Its application to both thin and thick guides indicates the central role played by the caustics in shaping the character of the propagation. Figures 3 and 6 illustrate the results we can obtain with this formulation.

At the same time a number of questions remain unanswered. Do the eigenmodes describing inplane elastic waves in an annulus constitute a complete

set? Do the eigenmodes for more general geometries constitute complete sets? What happens to the eigenmode structure when two eigenmodes are allowed to coalesce? What happens to the higher order terms in the asymptotic expansion described here when this happens? What is the correction, if any to the wavenumbers of the two lowest eigenmodes in a thin curved guide caused by the curvature alone. How do the Rayleigh-like waves transform into whispering gallery waves when the curvature becomes too large to permit the Rayleigh -like waves to exist? What does the wavefield in the Airy region look like[3] ?

We have made a beginning; much remains to be done.

Acknowledgements

This work was supported by the AFOSR, grant number F49620-96-1-0190, and the NSF grant number CMS-9812820. I thank both agencies. Closing parts of the work were done at the Department of Mathematics of the University of Manchester. I thank the Department for their hospitality. The conjectures posed and conclusions reached are my sole responsibility.

References

[1] J. G. Harris, Propagation in curved waveguides, in: I.D. Abrahams (ed.) Proceedings of the IUTAM Symposium on Diffraction and Scattering in Fluid Mechanics and Elasticity, Kluwer, Dordrecht, 2001.

[2] R. Grimshaw, Propagation of surface waves at high frequencies, J. Inst. Maths. Applics. 4 (1968) 174–193.

[3] R. D. Gregory, The propagation of Rayleigh waves over curved surfaces at high frequency, Proc. Camb. Phil. Soc. 70 (1971) 103–121.

[4] R. Smith, Asymptotic solutions for high-frequency trapped wave propagation, Phil. Trans. R. Soc. Lond. A 268 (1970) 289–324.

[5] R. Smith, Propagation in slowly-varying wave-guides, SIAM J. Appl. Math. 33 (1977) 39–50.

[6] R. Burridge, & H. Weinberg, Horizontal rays and vertical modes, in: J. B. Keller & J. S. Papadakis (eds.), Wave Propagation and Underwater Acoustics, Springer, New York (1977)

[3] Professor V. A. Borovikov suggested to me that an investigation of the wavefield in the Airy region may have been attempted.

[7] V. V. Krylov, Rayleigh waves on smooth surfaces of arbitrary shape, Sov. Phys. Acoust. 25 (1979) 425–428.

[8] I. A. Viktorov, Rayleigh-type waves on a cylindrical surface, Sov. Phys. Acoust. 4 (1958) 131–136.

[9] B. Rulf, Rayleigh waves on curved surfaces, J. Acoust. Soc. Am. 45 (1969) 493–499.

[10] L. M. Brekhovskikh, Surface waves confined to the curvature of the boundary in solids, Sov. Phys. Acoust. 13 (1968) 462–472.

[11] J. A. Morrison, Propagation of high frequency surface waves along cylinders of general cross section, J. Math. Phys. 16 (1975) 1786–1794.

[12] L. O. Wilson and J. A. Morrison, Propagation of high frequency elastic surface waves along cylinders of general cross-section, J. Math. Phys. 16 (1975) 1795–1805.

[13] D. S. Ahluwalia, J. B. Keller and B. J. Matkowsky, Asymptotic theory of propagation in curved and nonuniform waveguides, J. Acoust. Soc. Am. 55 (1974) 7–12.

[14] J. B. Keller and D. S. Ahluwalia, Uniform asymptotic solutions of eigenvalue problems for convex plane domains, SIAM J. Appl. Math. 25 (1975) 583–591.

[15] V. M. Babič and N. Y. Kirpičnikova, The Boundary-Layer Method in Diffraction Problems, Springer, Berlin, 1979.

[16] V. M. Babič and V. S. Buldyrev, Short-Wavelength Diffraction Theory, Springer, New York 1991.

[17] G. Liu and J. Qu, Guided circumferential waves in a circular annulus, J. Appl. Mech. 65 (1998) 424–430.

[18] G. Liu and J. Qu, Transient wave propagation in a circular annulus subjected to transient excitation on its outer surface, J. Acoust. Soc. Am. 104 (1998) 1210–1220.

[19] A. Folguera and J. G. Harris, Coupled Rayleigh surface waves in a slowly varying elastic waveguide, Proc. R. Soc. Lond. A 455 (1999) 917–931.

[20] F. W. J. Olver, Bessel functions of integer order, in: M. Abromowitz and I. A. Stegun (eds.) Handbook of Mathematical Functions, Dover, New York,1965.

[21] P. Kirrmann, On the completeness of Lamb modes, J. Elasticity 37 (1995) 39-69.

[22] B. A. Auld, Acoustic Fields and Waves in Solids, Vol. 2, Krieger, Malabar, Florida, 1990.

[23] F. B. Hildebrand, Methods of Applied Mathematics, Dover, New York, 1992.

List of Recent TAM Reports

No.	Authors	Title	Date
874	Short, M., and A. K. Kapila	Blow-up in semilinear parabolic equations with weak diffusion *Combustion Theory and Modeling* **2**, 283-291 (1998)	Dec. 1997
875	Riahi, D. N.	Analysis and modeling for a turbulent convective plume—*Mathematical and Computer Modeling* **28**, 57–63 (1998)	Jan. 1998
876	Stremler, M. A., and H. Aref	Motion of three point vortices in a periodic parallelogram—*Journal of Fluid Mechanics* **392**, 101-128 (1999)	Feb. 1998
877	Dey, N., K. J. Hsia, and D. F. Socie	On the stress dependence of high-temperature static fatigue life of ceramics	Feb. 1998
878	Brown, E. N., and N. R. Sottos	Thermoelastic properties of plain weave composites for multilayer circuit board applications	Feb. 1998
879	Riahi, D. N.	On the effect of a corrugated boundary on convective motion—*Journal of Theoretical and Applied Mechanics* **29**, 22–36 (2000)	Feb. 1998
880	Riahi, D. N.	On a turbulent boundary layer flow over a moving wavy wall	Mar. 1998
881	Riahi, D. N.	Vortex formation and stability analysis for shear flows over combined spatially and temporally structured walls—*Mathematical Problems in Engineering* **5**, 317–328 (1999)	June 1998
882	Short, M., and D. S. Stewart	The multi-dimensional stability of weak heat release detonations—*Journal of Fluid Mechanics* **382**, 109–135 (1999)	June 1998
883	Fried, E., and M. E. Gurtin	Coherent solid-state phase transitions with atomic diffusion: A thermomechanical treatment—*Journal of Statistical Physics* **95**, 1361–1427 (1999)	June 1998
884	Langford, J. A., and R. D. Moser	Optimal large-eddy simulation formulations for isotropic turbulence—*Journal of Fluid Mechanics* **398**, 321–346 (1999)	July 1998
885	Riahi, D. N.	Boundary-layer theory of magnetohydrodynamic turbulent convection—*Proceedings of the Indian National Academy (Physical Science)* **65A**, 109–116 (1999)	Aug. 1998
886	Riahi, D. N.	Nonlinear thermal instability in spherical shells—in *Nonlinear Instability, Chaos and Turbulence* **2**, 377–402 (1999)	Aug. 1998
887	Riahi, D. N.	Effects of rotation on fully non-axisymmetric chimney convection during alloy solidification—*Journal of Crystal Growth* **204**, 382–394 (1999)	Sept. 1998
888	Fried, E., and S. Sellers	The Debye theory of rotary diffusion—*Archive for Rational Mechanics and Analysis*, in press (2000)	Sept. 1998
889	Short, M., A. K. Kapila, and J. J. Quirk	The hydrodynamic mechanisms of pulsating detonation wave instability—*Proceedings of the Royal Society of London, A* **357**, 3621–3638 (1999)	Sept. 1998
890	Stewart, D. S.	The shock dynamics of multidimensional condensed and gas phase detonations—Proceedings of the 27th International Symposium on Combustion (Boulder, Colo.)	Sept. 1998
891	Kim, K. C., and R. J. Adrian	Very large-scale motion in the outer layer—*Physics of Fluids* **2**, 417–422 (1999)	Oct. 1998
892	Fujisawa, N., and R. J. Adrian	Three-dimensional temperature measurement in turbulent thermal convection by extended range scanning liquid crystal thermometry—*Journal of Visualization* **1**, 355–364 (1999)	Oct. 1998
893	Shen, A. Q., E. Fried, and S. T. Thoroddsen	Is segregation-by-particle-type a generic mechanism underlying finger formation at fronts of flowing granular media?—*Particulate Science and Technology* **17**, 141–148 (1999)	Oct. 1998
894	Shen, A. Q.	Mathematical and analog modeling of lava dome growth	Oct. 1998
895	Buckmaster, J. D., and M. Short	Cellular instabilities, sub-limit structures, and edge-flames in premixed counterflows—*Combustion Theory and Modeling* **3**, 199–214 (1999)	Oct. 1998
896	Harris, J. G.	*Elastic waves*—Part of a book to be published by Cambridge University Press	Dec. 1998
897	Paris, A. J., and G. A. Costello	Cord composite cylindrical shells	Dec. 1998

List of Recent TAM Reports (cont'd)

No.	Authors	Title	Date
898	Students in TAM 293–294	Thirty-fourth student symposium on engineering mechanics (May 1997), J. W. Phillips, coordinator: Selected senior projects by M. R. Bracki, A. K. Davis, J. A. (Myers) Hommema, and P. D. Pattillo	Dec. 1998
899	Taha, A., and P. Sofronis	A micromechanics approach to the study of hydrogen transport and embrittlement	Jan. 1999
900	Ferney, B. D., and K. J. Hsia	The influence of multiple slip systems on the brittle–ductile transition in silicon—*Materials Science Engineering A* **272**, 422–430 (1999)	Feb. 1999
901	Fried, E., and A. Q. Shen	Supplemental relations at a phase interface across which the velocity and temperature jump—*Continuum Mechanics and Thermodynamics* **11**, 277–296 (1999)	Mar. 1999
902	Paris, A. J., and G. A. Costello	Cord composite cylindrical shells: Multiple layers of cords at various angles to the shell axis	Apr. 1999
903	Ferney, B. D., M. R. DeVary, K. J. Hsia, and A. Needleman	Oscillatory crack growth in glass—*Scripta Materialia* **41**, 275–281 (1999)	Apr. 1999
904	Fried, E., and S. Sellers	Microforces and the theory of solute transport—*Zeitschrift für angewandte Mathematik und Physik* **51**, 732–751 (2000)	Apr. 1999
905	Balachandar, S., J. D. Buckmaster, and M. Short	The generation of axial vorticity in solid-propellant rocket-motor flows	May 1999
906	Aref, H., and D. L. Vainchtein	The equation of state of a foam—*Physics of Fluids* **12**, 23–28 (2000)	May 1999
907	Subramanian, S. J., and P. Sofronis	Modeling of the interaction between densification mechanisms in powder compaction	May 1999
908	Aref, H., and M. A. Stremler	Four-vortex motion with zero total circulation and impulse—*Physics of Fluids* **11**, 3704-3715	May 1999
909	Adrian, R. J., K. T. Christensen, and Z.-C. Liu	On the analysis and interpretation of turbulent velocity fields—*Experiments in Fluids* **29**, 275–290 (2000)	May 1999
910	Fried, E., and S. Sellers	Theory for atomic diffusion on fixed and deformable crystal lattices—*Journal of Elasticity*, in press (2000)	June 1999
911	Sofronis, P., and N. Aravas	Hydrogen induced shear localization of the plastic flow in metals and alloys	June 1999
912	Anderson, D. R., D. E. Carlson, and E. Fried	A continuum-mechanical theory for nematic elastomers—*Journal of Elasticity* **56**, 33–58 (1999)	June 1999
913	Riahi, D. N.	High Rayleigh number convection in a rotating melt during alloy solidification—*Recent Developments in Crystal Growth Research* **2**, 211–222 (2000)	July 1999
914	Riahi, D. N.	Buoyancy driven flow in a rotating low Prandtl number melt during alloy solidification—*Current Topics in Crystal Growth Research*, in press (2000)	July 1999
915	Adrian, R. J.	On the physical space equation for large-eddy simulation of inhomogeneous turbulence	July 1999
916	Riahi, D. N.	Wave and vortex generation and interaction in turbulent channel flow between wavy boundaries	July 1999
917	Boyland, P. L., M. A. Stremler, and H. Aref	Topological fluid mechanics of point vortex motions	July 1999
918	Riahi, D. N.	Effects of a vertical magnetic field on chimney convection in a mushy layer—*Journal of Crystal Growth* **216**, 501–511 (2000)	Aug. 1999

List of Recent TAM Reports (cont'd)

No.	Authors	Title	Date
919	Riahi, D. N.	Boundary mode–vortex interaction in turbulent channel flow over a non-wavy rough wall	Sept. 1999
920	Block, G. I., J. G. Harris, and T. Hayat	Measurement models for ultrasonic nondestructive evaluation	Sept. 1999
921	Zhang, S., and K. J. Hsia	Modeling the fracture of a sandwich structure due to cavitation in a ductile adhesive layer	Sept. 1999
922	Nimmagadda, P. B. R., and P. Sofronis	Leading order asymptotics at sharp fiber corners in creeping-matrix composite materials	Oct. 1999
923	Yoo, S., and D. N. Riahi	Effects of a moving wavy boundary on channel flow instabilities	Nov. 1999
924	Adrian, R. J., C. D. Meinhart, and C. D. Tomkins	Vortex organization in the outer region of the turbulent boundary layer	Nov. 1999
925	Riahi, D. N., and A. T. Hsui	Finite amplitude thermal convection with variable gravity—*International Journal of Mathematics and Mathematical Sciences*, in press (2000)	Dec. 1999
926	Kwok, W. Y., R. D. Moser, and J. Jiménez	A critical evaluation of the resolution properties of *B*-spline and compact finite difference methods	Feb. 2000
927	Ferry, J. P., and S. Balachandar	A fast Eulerian method for two-phase flow	Feb. 2000
928	Thoroddsen, S. T., and K. Takehara	The coalescence–cascade of a drop	Feb. 2000
929	Liu, Z.-C., R. J. Adrian, and T. J. Hanratty	Large-scale modes of turbulent channel flow: Transport and structure	Feb. 2000
930	Borodai, S. G., and R. D. Moser	The numerical decomposition of turbulent fluctuations in a compressible boundary layer	Mar. 2000
931	Balachandar, S., and F. M. Najjar	Optimal two-dimensional models for wake flows	Mar. 2000
932	Yoon, H. S., K. V. Sharp, D. F. Hill, R. J. Adrian, S. Balachandar, M. Y. Ha, and K. Kar	Integrated experimental and computational approach to simulation of flow in a stirred tank	Mar. 2000
933	Sakakibara, J., Hishida, K., and W. R. C. Phillips	On the vortical structure in a plane impinging jet	Apr. 2000
934	Phillips, W. R. C.	Eulerian space–time correlations in turbulent shear flows	Apr. 2000
935	Hsui, A. T., and D. N. Riahi	Onset of thermal–chemical convection with crystallization within a binary fluid and its geological implications	Apr. 2000
936	Cermelli, P., E. Fried, and S. Sellers	Configurational stress, yield, and flow in rate-independent plasticity—*Proceedings of the Royal Society of London A* (submitted)	Apr. 2000
937	Adrian, R. J., C. Meneveau, R. D. Moser, and J. J. Riley	Final report on 'Turbulence Measurements for Large-Eddy Simulation' workshop	Apr. 2000
938	Bagchi, P., and S. Balachandar	Linearly varying ambient flow past a sphere at finite Reynolds number—Part 1: Wake structure and forces in steady straining flow	Apr. 2000
939	Gioia, G., A. DeSimone, M. Ortiz, and A. M. Cuitiño	Folding energetics in thin-film diaphragms	Apr. 2000
940	Chaïeb, S., and G. H. McKinley	Mixing immiscible fluids: Drainage induced cusp formation	May 2000

List of Recent TAM Reports (cont'd)

No.	Authors	Title	Date
941	Thoroddsen, S. T., and A. Q. Shen	Granular jets	May 2000
942	Riahi, D. N.	Non-axisymmetric chimney convection in a mushy layer under a high-gravity environment—In *Centrifugal Materials Processing* (L. L. Regel and W. R. Wilcox, eds.), in press (2000)	May 2000
943	Christensen, K. T., S. M. Soloff, and R. J. Adrian	PIV Sleuth: Integrated particle image velocimetry interrogation/validation software	May 2000
944	Wang, J., N. R. Sottos, and R. L. Weaver	Laser induced thin film spallation	May 2000
945	Riahi, D. N.	Magnetohydrodynamic effects in high gravity convection during alloy solidification—In *Centrifugal Materials Processing* (L. L. Regel and W. R. Wilcox, eds.), in press (2000)	June 2000
946	Gioia, G., Y. Wang, and A. M. Cuitiño	The energetics of heterogeneous deformation in open-cell solid foams	June 2000
947	Kessler, M. R., and S. R. White	Self-activated healing of delamination damage in woven composites—*Composites A*, in press (2000)	June 2000
948	Phillips, W. R. C.	On the pseudomomentum and generalized Stokes drift in a spectrum of rotational waves	July 2000
949	Hsui, A. T., and D. N. Riahi	Does the Earth's nonuniform gravitational field affect its mantle convection?	July 2000
950	Phillips, J. W.	Abstract Book, 20th International Congress of Theoretical and Applied Mechanics (27 August – 2 September, 2000, Chicago)	July 2000
951	Vainchtein, D. L., and H. Aref	Morphological transition in compressible foam	July 2000
952	Chaïeb, S., E. Sato-Matsuo, and T. Tanaka	Shrinking-induced instabilities in gels	July 2000
953	Riahi, D. N., and A. T. Hsui	A theoretical investigation of high Rayleigh number convection in a nonuniform gravitational field	Aug. 2000
954	Riahi, D. N.	Effects of centrifugal and Coriolis forces on a hydromagnetic chimney convection in a mushy layer	Aug. 2000
955	Fried, E.	An elementary molecular-statistical basis for the Mooney and Rivlin–Saunders theories of rubber-elasticity—*Journal of the Mechanics and Physics of Solids*, to appear	Sept. 2000
956	Phillips, W. R. C.	On an instability to Langmuir circulations and the role of Prandtl and Richardson numbers	Sept. 2000
957	Chaïeb, S., and J. Sutin	Growth of myelin figures made of water soluble surfactant—Proceedings of the 1st Annual International IEEE–EMBS Conference on Microtechnologies in Medicine and Biology (October 2000, Lyon, France), 345–348	Oct. 2000
958	Christensen, K. T., and R. J. Adrian	Statistical evidence of hairpin vortex packets in wall turbulence—*Journal of Fluid Mechanics*, to appear	Oct. 2000
959	Kuznetsov, I. R., D. S. Stewart, and E. Fried	Modeling the thermal expansion boundary layer during the combustion of energetic materials—*Combustion and Flame* (submitted)	Oct. 2000
960	Zhang, S., K. J. Hsia, and A. J. Pearlstein	Potential flow model of cavitation-induced interfacial fracture in a confined ductile layer—*Journal of the Mechanics and Physics of Solids* (submitted)	Nov. 2000
961	Sharp, K. V., R. J. Adrian, J. G. Santiago, and J. I. Molho	Liquid flows in microchannels—Chapter 6 of *CRC Handbook of MEMS* (M. Gad-el-Hak, ed.) (2001)	Nov. 2000
962	Harris, John G.	Rayleigh wave propagation in curved waveguides—Elsevier preprint (submitted)	Jan. 2001